



Significant enhancement in $\text{Eu}^{3+}/\text{Eu}^{2+}$ emissions intensity by CdS quantum dots, in chloroborosilicate glasses

Nilanjana Shasmal^{a,*}, Walter José Gomes Juste Faria^b, Andrea Simone Stucchi de Camargo^b, Ana Candida Martins Rodrigues^a

^a Universidade Federal de São Carlos, Departamento de Engenharia de Materiais, LaMaV - Laboratório de Materiais Vítreatos, Rod. Washington Luiz, km 235, 13565-905, São Carlos, SP, Brazil

^b São Carlos Institute of Physics, LEMAF – Laboratório de Espectroscopia de Materiais Funcionais, University of São Paulo, Avenida Trabalhador São-Carlense, nº 400 Parque Arnold Schimidt, CEP 13566-590, São Carlos, SP, Brazil

ARTICLE INFO

Keywords:

CdS quantum Dots
Eu/CdS co-Doped glass
 $\text{Eu}^{3+}/\text{Eu}^{2+}$ emission
Energy transfer
Enhanced emission
Chloroborosilicate glass

ABSTRACT

Eu^{3+} and CdS were singly doped and co-doped into chloroborosilicate glasses with composition $37.8\text{SiO}_2-27\text{B}_2\text{O}_3-18\text{BaO}-3.6\text{K}_2\text{O}-3.6\text{Al}_2\text{O}_3-10\text{BaCl}_2$ (mol%), by one-step melt quench technique. The samples were characterized by transmission electron microscopy (TEM), UV-Vis absorption, excitation, and emission spectroscopy. TEM images revealed the presence of CdS quantum dots (QDs) of size 5–20 nm in the CdS-doped glasses. The Eu-doped glass shows characteristic orange emission of Eu^{3+} at 393 nm excitation, while excitation at 250 and 317 nm revealed the existence of Eu^{2+} ions. There are strong evidences of energy transfer involving the charge transfer band (CTB) and different energy levels of Eu^{2+} and Eu^{3+} ions. The CdS-doped glass showed broad emission bands, originating from various electronic transitions involving defect and trap states in CdS crystalline structure. The emission band in the lower wavelength region, shows a red shift with increasing excitation wavelength, which proves the quantum confinement effect in CdS QDs. Eu/CdS co-doped glasses showed significant enhancements in $\text{Eu}^{3+}/\text{Eu}^{2+}$ emissions, up to 20 and 70 times, upon excitations at 393 and 317 nm, respectively, which is considerably higher compared to previously reported similar systems. This enhancement is attributed to a complex energy transfer occurring between $\text{Eu}^{2+}/\text{Eu}^{3+}$ and CdS QDs, reported for the first time in a glassy system, especially considering the in-situ growth of the QDs during melt. The co-doped glass also showed pure white emission at 6–7 nm slit width upon 387 nm excitation, which is a novel finding from an Eu/CdS co-doped glass.

1. Introduction

Semiconductor quantum dots (QDs), one of the most important nanomaterials for applications in diverse fields of photonics, are a subject of considerable interest given their unique optical properties and functionalities, due to quantum confinement effects, which are not exhibited by their bulk counterparts [1–3]. Recently, photochemically stable II-VI semiconductors (ZnSe, CdS, CdSe, etc) QDs have played a substantial role as luminescent materials, with tunable emissions associated with their size-dependent band gap. These characteristics lead to several advantages in optical applications, such as higher absorption cross-section, and narrow, tunable and Stokes shifted emission spectra [4,5]. CdS is one of the most common II-VI semiconductor QDs, and it can emit over a wide range of wavelengths depending on the dots size. As an increasingly important wide-bandgap (2.42 eV) material, it has been used in many applications such as ultraviolet light-emitting diodes

and injection lasers, flat-panel displays, electroluminescent devices and infrared windows, etc. [6–8].

In general, stabilization of nanometer-sized particles is difficult, particularly when embedded in unsuitable host materials, with poor thermal resistance. When exposed to high temperature, which might be a consequence of high-power excitation, heating effects may result in the degradation of photoluminescence efficiency, and a decrease in the lifespan of the luminescent device [4]. Therefore, in the last decade, efforts have been made to find suitable, hosts matrices for the incorporation of QDs and, among them, some glasses have proven to be excellent choices given their high thermal resistance and transparency for visible light emission [9]. The study of CdS-doped glasses is motivated by the extended use of CdS as a phosphor, in photovoltaic cells, field effect transistors, heterojunction lasers, acoustic amplifiers, etc [4–9]. Several publications concerning CdS doped silica [10,11] or zirconia [12] prepared by the sol-gel technique, have appeared in recent years.

* Corresponding author.

E-mail address: nilanjana1508@gmail.com (N. Shasmal).

In order to tune their emission wavelength, different rare earth elements (Ho^{3+} , Eu^{3+} , Er^{3+} , etc) are often co-doped into II-VI semiconductor QDs (CdS, ZnS, ZnSe, etc) altering the emission recombination processes [13–16]. Rare earth ions present a unique 4f electronic structure leading to 4f–4f or 5d–4f transitions which can introduce new fluorescence characteristics to II-VI QDs [17,18]. Europium (Eu) is the most commonly used element, because the Eu doped QDs have a wide emission band and tunable emission colors ranging from blue to red, very suitable for applications in white LEDs [19]. Several authors have reported that the luminescence of Eu^{3+} ions can be efficiently enhanced by co-doping Eu^{3+} with CdS QDs in a suitable host matrix, so that energy transfer from the QDs to the Eu^{3+} ions takes place [19–23]. Similar observations were reported in several other Eu^{3+} -CdS systems, prepared by sol-gel technique [24,25] or in thin films prepared by chemical spray pyrolysis [26]. However, reports of glasses co-doped with Eu^{3+} and CdS QDs, obtained by melt-quenching technique are also rare.

In view of the above introduction, we present a study of the obtainment and structural and spectroscopic characterization of a new glass system co-doped with Eu^{3+} and CdS QDs obtained by the conventional melt-quenching technique. Chloroborosilicate (CBS) glasses - a modified version of borosilicate glasses [27] with general composition (mol%) $(100-x)(42\text{SiO}_2-30\text{B}_2\text{O}_3-20\text{BaO}-4\text{K}_2\text{O}-4\text{Al}_2\text{O}_3)-x\text{BaCl}_2$ (where $x = 0-30$), have been previously reported as excellent host matrices for rare earth ions like Sm^{3+} and Dy^{3+} and metal (Ag and Au) NPs [28–30]. Considerable enhancement in the RE emissions have been observed in presence of the surface plasmon resonance effect of Ag and Au NPs, in this glass matrix [28–30]. So, there should be a fair possibility that the same kind of enhancement effect can be obtained in this glass if co-doped with RE/semiconductor QDs. The glass is thermally stable and also remains transparent over a prolonged period of heating treatment (up to 120 h at 680 °C) [31]. Based on this previous knowledge, in the present study, Eu^{3+} and CdS were doped separately and co-doped into a chloroborosilicate glasses, with composition $37.8\text{SiO}_2-27\text{B}_2\text{O}_3-18\text{BaO}-3.6\text{K}_2\text{O}-3.6\text{Al}_2\text{O}_3-10\text{BaCl}_2$ (mol%), through the one-step melt-quenching technique. The resulting transparent samples were characterized by transmission electron microscopy (TEM) and absorption, excitation and emission spectroscopies. A significant emission enhancement was observed due to several energy transfer mechanisms.

2. Experimental procedure

2.1. Samples preparation

The employed raw materials were quartz (SiO_2), boric acid (H_3BO_3),

barium carbonate (BaCO_3), potassium carbonate (K_2CO_3), aluminum oxide (Al_2O_3) barium chloride (BaCl_2), europium oxide (Eu_2O_3) and cadmium sulfide (CdS), all purchased from AR, Sigma Aldrich. They were used directly without any further purification. Glass batches of 70 g, with the compositions depicted in Table 1, were prepared by melting homogeneous mixtures of the powders with calculated composition in a high-purity alumina crucible at 1250 °C for 1.5 h, intermittently stirring with a silica rod for 0.5 min in air in a raising hearth electric furnace. The crucible was covered with an alumina lid during the melting process. The molten samples were cast into an iron plate in air and annealed at 600 °C for 6 h in order to remove the residual thermal stresses, followed by slow cooling down to room temperature. The glass pieces were cut and polished for optical characterizations.

2.2. Characterization

The base glass had been previously characterized by differential scanning calorimetry (DSC), X-ray diffraction (XRD), scanning electron microscopy (SEM), transmission electron microscopy (TEM) and energy dispersive X-Ray analysis (EDX) [27–31]. The glass transition temperature of the glass was found to be 634 °C [27], the glass was amorphous when prepared, but BaCl_2 nanocrystals were found to develop with heat treatment at 650 °C, as confirmed by SEM and TEM studies [28–31]. In the present study, the microstructures were analyzed by TEM, EDX, and selected area electron diffraction (SAED) using a MEV XL30 FEG microscope. To investigate the spectroscopic properties, the samples were cut into pieces of the same size and thickness (15 mm × 15 mm × 5 mm), and polished using sandpapers of different grades. The absorption spectra were measured in a PerkinElmer UV–Vis–NIR spectrophotometer model Lambda 950, working on the double beam principle. In this equipment, the source consists of a deuterium lamp for the UV spectral region and a tungsten lamp for the visible to infrared region. The PL excitation and emission spectra were collected in a HORIBA Jobin Yvon spectrofluorimeter model Fluorolog FL3-221, equipped with a CW xenon flash lamp and a visible photodetector (HORIBA PPD-850). To avoid overlapping of different orders of diffracted radiation, optical filters were employed in the path of the source beam.

3. Results and discussion

3.1. Transmission electron microscopy

Fig. 1 (a) and (b) show representative TEM images of sample CdS10 and Eu10_CdS30. Spherical particles with sizes ranging from 5 to 20 nm

Table 1

Eu_2O_3 and CdS content (wt % in excess) in the base glass composition: $37.8\text{SiO}_2-27\text{B}_2\text{O}_3-18\text{BaO}-3.6\text{K}_2\text{O}-3.6\text{Al}_2\text{O}_3-10\text{BaCl}_2$ (mol%).

Sample no	Sample ID	Eu_2O_3 (wt%)	CdS (wt%)	Colour
1	Eu10	1	-	Colorless
2	CdS10	-	1	Yellow
3	Eu10_CdS10	1	1	Light yellow
4	Eu10_CdS20	1	2	Light yellow
5	Eu10_CdS30	1	3	Light yellow
6	Eu10_CdS50	1	5	Light yellow



Photographs of the prepared samples, left to right, Eu10, CdS10, Eu10_CdS10, Eu10_CdS20, Eu10_CdS30 and Eu10_CdS50

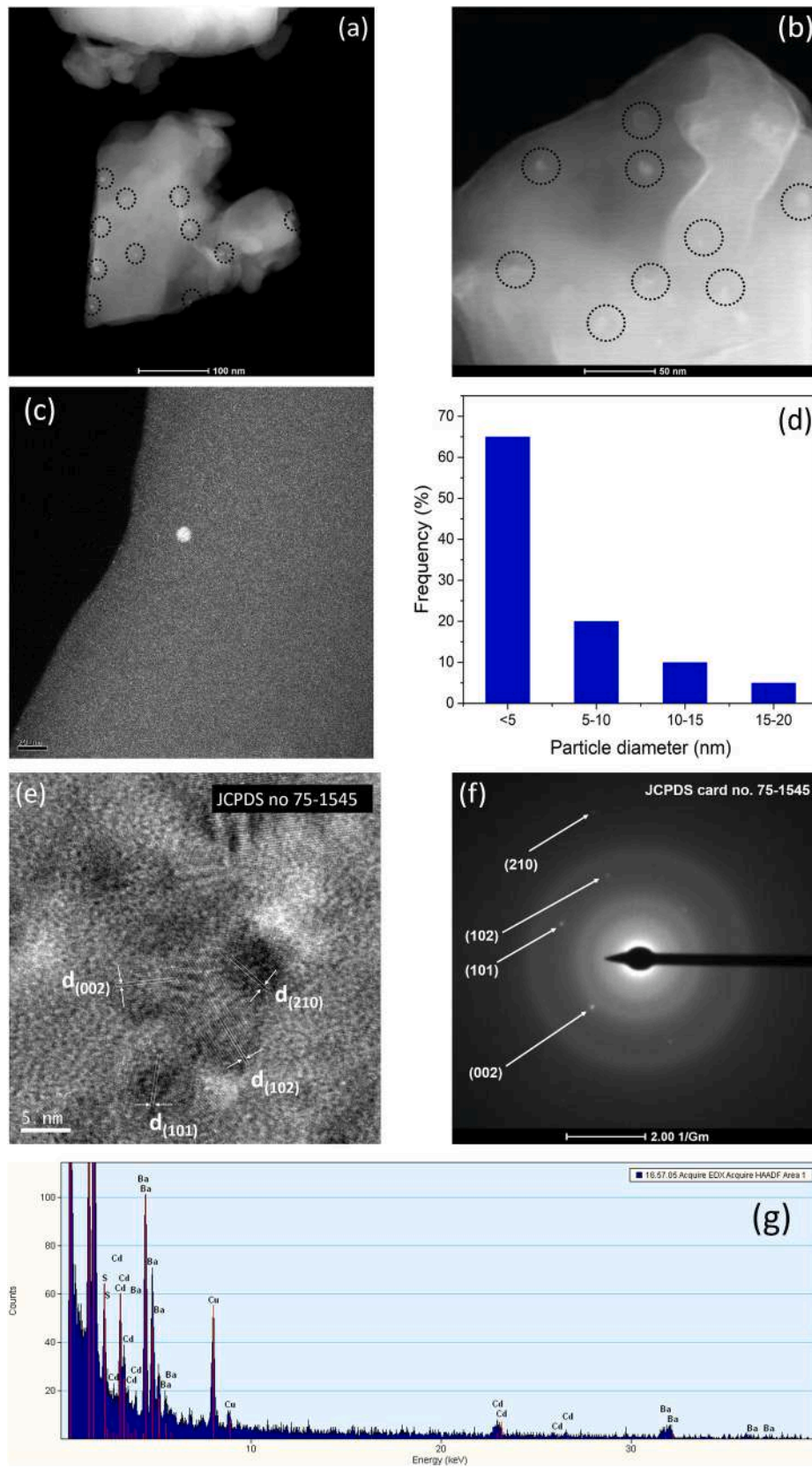


Fig. 1. Representative TEM images of (a) CdS10, (b) Eu10CdS30, (c) high resolution TEM image of CdS10, (d) particle size distribution histogram of CdS10, (e) HRTEM of CdS10, (f) SAED pattern of CdS10, showing different crystalline planes of CdS, (g) EDX spectrum of CdS10.

Table 2
Quantitative analysis by EDX of CdS10 sample.

Element	Weight %	Atomic %	Error %	Correction	k-Factor
O(K)	62.30	78.09	0.45	0.49	1.974
Al(K)	3.34	2.49	0.07	0.92	1.027
Si(K)	23.66	16.95	0.19	0.92	1.000
S(K)	0.28	0.05	0.01	0.93	1.021
Cl(K)	0.34	0.03	0.09	0.95	1.063
Cd(K)	0.68	0.12	0.09	0.97	7.185
Ba(K)	9.40	1.37	0.26	0.89	14.877

can be observed in both samples. Most of the observable particles are below 10 nm size, a few of them are bigger. Fig. 1(c) represents a high-resolution image of sample CdS10, zooming over one single spherical particle with a diameter lower than 10 nm. Fig. 1(d) shows a histogram presenting the particle size distribution of CdS QDs in the sample CdS10. It shows that more than 60% of the particles are smaller than 5 nm in diameter. Fig. 1 (e) shows a HRTEM image of the same sample showing different crystalline planes of CdS crystal, planes have been identified and assigned with JCPDS no. 75–1545. Fig. 1 (f) shows the selected area electron diffraction (SAED) pattern of this particular particle. The presence of multiple rings represents different crystalline planes. The d-spacing values have been calculated and they match with the d-spacings of different crystal planes (101), (102), (002) and (210) of CdS crystal (JCPDS no. 75–1545). This confirms the presence of CdS nanoparticles in the prepared glasses. Energy dispersive X-ray (EDX) analysis was also performed on the same area of the same CdS10 sample. Fig. 1(g) shows the EDX spectrum of the same representative sample. It shows Cd and S peaks which again confirm the presence of CdS in the sample. Table 2 shows the weight percentage of every element present in the sample. Cd and S are present in significant amounts. The alumina content is slightly higher (3.34 wt%) than it should be according to the glass composition (~3 wt%). This is probably due to the inclusion from the alumina crucible during melting.

3.2. Absorption spectra

The absorption spectrum of Eu10 in the UV–visible range is presented in Fig. 2(a). The spectrum reveals the ground state absorption bands of Eu^{3+} ion corresponding to the transitions ${}^7\text{F}_0 \rightarrow {}^5\text{D}_2$ (464 nm),

${}^7\text{F}_0 \rightarrow {}^5\text{L}_6$ (393 nm), and ${}^7\text{F}_0 \rightarrow {}^5\text{D}_4$ (362 nm), assigned in accordance with Carnal's convention [32,33].

As shown in Fig. 2(b), the absorption spectrum of CdS10 shows a broad absorption band starting from 500 nm (green region) and centered around 400 nm (violet region). For wavelength below 400 nm, the absorption reaches saturation, which indicates that the glass reaches its UV cut-off wavelength. The spectra of Eu/CdS co-doped glasses show the characteristics of both Eu^{3+} and CdS QDs, i.e. the sharp absorption peaks at 393 and 464 nm and a progressive broad band starting around 500 nm.

3.3. Emission and excitation spectra

3.3.1. Emission and excitation spectra of Eu10 sample

All of the Eu-containing glasses present bright red emission when excited at 393 (${}^7\text{F}_0 \rightarrow {}^5\text{L}_6$) and 464 nm (${}^7\text{F}_0 \rightarrow {}^5\text{D}_2$). Fig. 3(a) depicts the representative photoluminescence spectrum of Eu10 obtained upon excitation at 393 nm. The spectrum exhibits characteristic emission peaks between 570 nm and 720 nm assigned to transitions within the $4f^6$ configuration of Eu^{3+} . The dominant intense red emission at 612 nm corresponds to the hypersensitive ${}^5\text{D}_0 \rightarrow {}^7\text{F}_2$ forced electric-dipole transition. The other emission peaks have been assigned to ${}^5\text{D}_0 \rightarrow {}^7\text{F}_0$ (579 nm), ${}^5\text{D}_0 \rightarrow {}^7\text{F}_1$ (591 nm), ${}^5\text{D}_0 \rightarrow {}^7\text{F}_3$ (652 nm), and ${}^5\text{D}_0 \rightarrow {}^7\text{F}_4$ (703 nm) transitions of the Eu^{3+} ions. The inset of the figure clearly demonstrates the bright red luminescence under 393 nm excitation. The same emission bands appear when excited at 464 nm.

The excitation spectra were recorded by monitoring the Eu^{3+} emission at 612 nm (${}^5\text{D}_0 \rightarrow {}^7\text{F}_2$) for all the Eu-containing samples. All of them display similar nature as represented by the excitation spectrum of Eu10 shown in Fig. 3(b). Sharp peaks have been revealed in 300–600 nm wavelength range corresponding to transitions from the ground state to the excited states within the $4f^6$ configuration of Eu^{3+} as duly assigned. A sharp rise in intensity, was observed in the range 300 to 250 nm which could not be investigated beyond 250 nm due to experimental limitations. This intense broad band corresponds to the charge transfer band (CTB) of Eu.

Fig. 4(a) depicts the photoluminescence spectra of Eu10 obtained upon excitation at 305 nm (${}^7\text{F}_0 \rightarrow {}^5\text{H}_6$). The spectra exhibit sharp peaks in the wavelength range 570–720 nm along with an intense broad emission band peaking at 430 nm. The sharp peaks in the longer

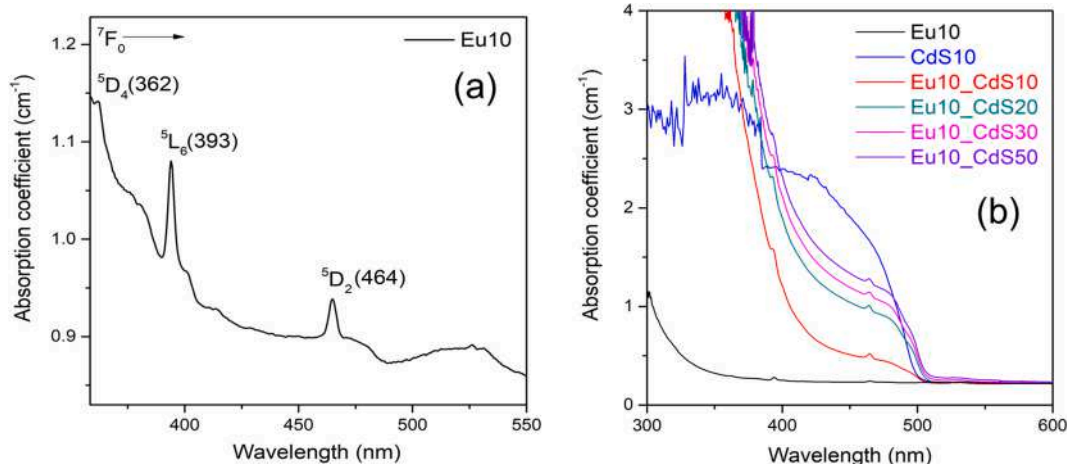


Fig. 2. UV–Vis absorption spectra of (a) Eu10, indicating the characteristic transitions of Eu^{3+} ; (b) all the prepared samples.

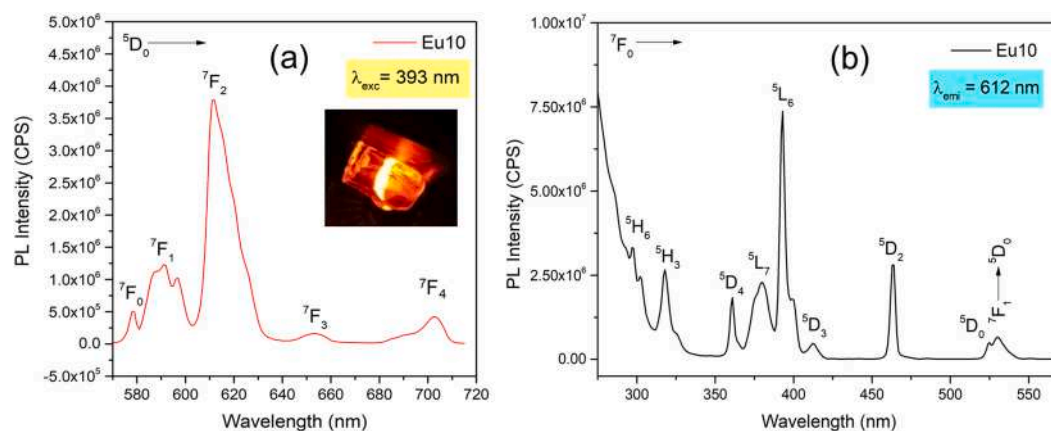


Fig. 3. (a) Emission spectra of Eu10 with excitations at 393 nm, (the inset shows a photograph of the emitting sample), (b) Excitation spectra of Eu10 monitoring the emission at 612 nm.

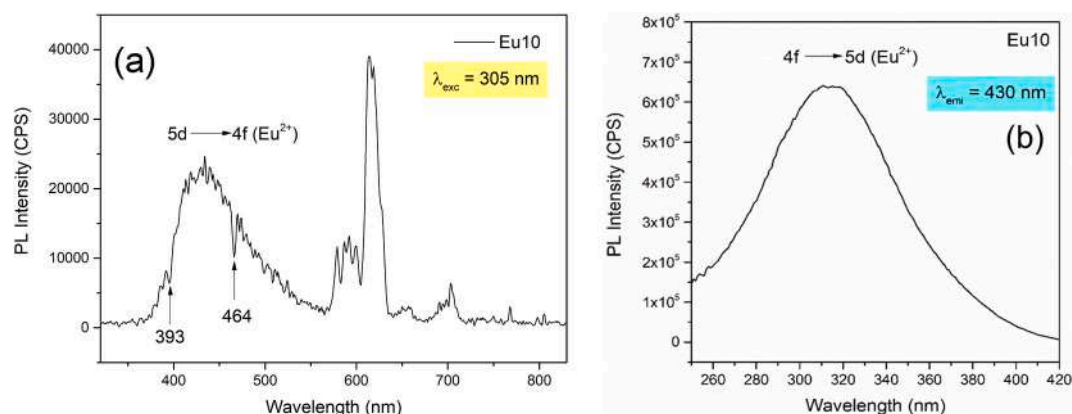


Fig. 4. (a) Emission spectra of Eu10 with excitations at 305 nm, (b) Excitation spectra of Eu10 monitoring the emission at 430 nm.

wavelengths have been assigned to $^5D_0 \rightarrow ^7F_{0-4}$ of Eu^{3+} ions. The broad emission band may be attributed to the characteristic $4f^65d \rightarrow 4f^7$ transition of Eu^{2+} ions [34]. To investigate the origin of the broad emission band in the blue region, an excitation spectrum was taken monitoring the emission at 430 nm, as illustrated in Fig. 4(b). The spectrum shows a broad excitation band in the range of 280–380 nm, peaking around 317 nm, which indeed reveals the characteristic $4f \rightarrow 5d$ transition of Eu^{2+} . The same trends were observed in all the Eu-containing samples. This clearly establishes the existence of Eu^{2+} ions in all the Eu-doped samples.

On the broad emission band of Eu10 in Fig. 4(a), there are two visible holes located at 393 and 464 nm, which correspond to the two most prominent, characteristic absorptions of Eu^{3+} . As it is understood that the broad emission band originates from the $4f^65d \rightarrow 4f^7$ transition of Eu^{2+} ions, the presence of those two holes clearly indicates that there is energy transfer taking place from Eu^{2+} to Eu^{3+} ions. This kind of energy transfer is not uncommon in the case of systems containing both the divalent and trivalent ions [35,36].

In the excitation spectra measured monitoring the emission at 612 nm (Fig. 3(b)), the sharp rise, observed below 300 nm, corresponds to the charge transfer band (CTB) of Eu. When excited at any wavelengths between 250 and 290 nm, it resulted in the intense emission at 612 nm, characteristic for Eu^{3+} along with the other emission bands at longer wavelengths and the broad band from 380 to 500 nm peaking at 430 nm,

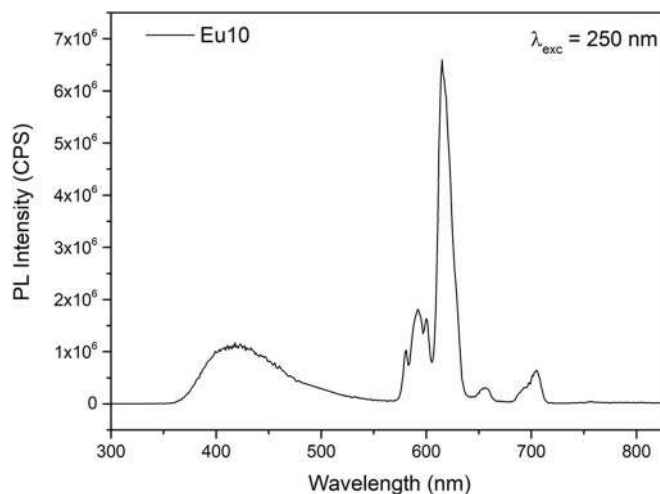


Fig. 5. Emission spectra of Eu10 with excitations at 250 nm.

characteristic for Eu^{2+} [35,36], as shown in Fig. 5.

These evidences corroborate the presence of both Eu^{2+} and Eu^{3+} ions in the europium doped CBS glass and also the energy transfer mechanism between them. Fig. 6 presents a schematic energy level diagram of

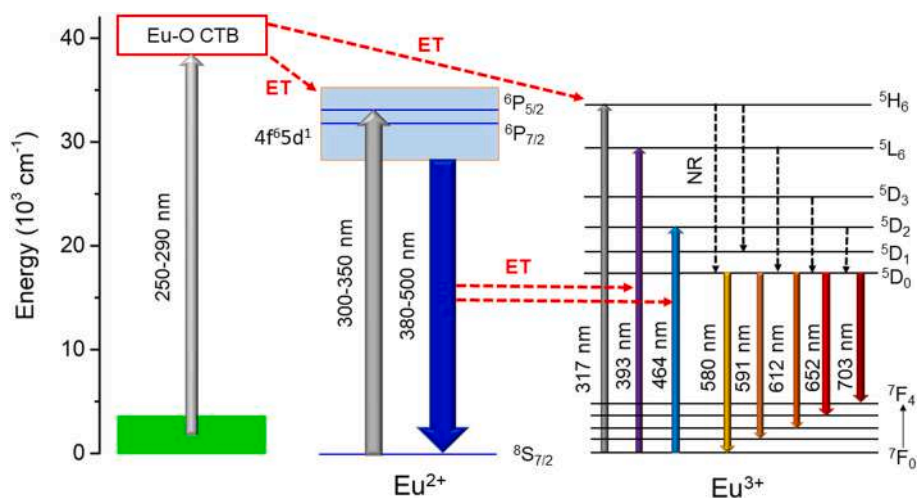


Fig. 6. Schematic energy level diagram of Eu^{2+} and Eu^{3+} showing the plausible electronic transitions and energy transfer mechanisms between them [based on Ref 36–38].

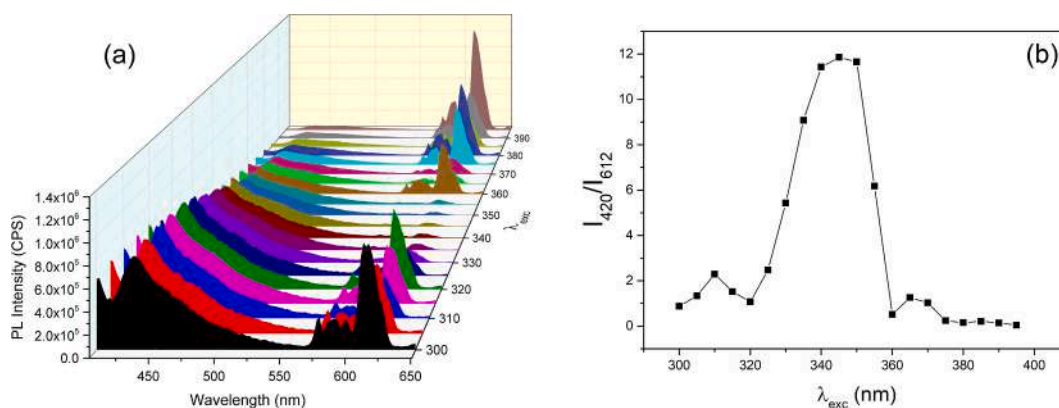


Fig. 7. (a) 3D Emission spectra of Eu10 at different excitation wavelengths from 300 to 395 nm, (b) Intensity ratio variation of emission bands at 420 and 612 nm as a function of different excitation wavelengths.

Eu^{2+} and Eu^{3+} showing the electronic transitions and energy transfer mechanisms, leading to the observed emission properties. Under 250–290 nm excitation, the Eu^{3+} ions are excited to the CT (charge transfer) state, and then decay to the 4f levels of Eu^{2+} and Eu^{3+} ions. Then both species decay to the lower vibrational energy levels and undergo radiative emissions.

The excitation spectrum shown in Fig. 4(b), exhibits a broad band, which is assigned to Eu^{2+} ($4f^7, {}^8S_{7/2} \rightarrow 4f^6 5d^1$). The broad band allows excitation of the glasses in the 300–350 nm [38] yielding a broad emission band in the range of 380–500 nm, which overlaps with the absorption region of Eu^{3+} [36–38].






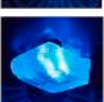





The confirmed presence of both divalent and trivalent Eu ions leads to strong emission bands in the blue (around 380–500 nm) and red region (612 nm) of the spectrum. The ratio of these bands varies considerably with the excitation wavelength. Fig. 7 (a) shows the variation of PL spectra of Eu10 at different excitations in the range of 300–395 nm. From the figure, it can be observed that at 300 nm excitation, both the emissions are intense, because both Eu^{2+} and Eu^{3+} are excited in the range 300–305 nm. With increasing excitation wavelength, the emission in the blue becomes more intense than the one in the red. From 340 to 350 nm, the blue band is predominant, whereas from 360 nm onwards, the red emission gets stronger and predominates, eventually yielding

maximum intensity at 612 nm, upon 395 nm excitation. Fig. 7 (b) shows the variation of the intensity ratio of the blue (380–500 nm) and red (612 nm) emission bands with different excitation wavelengths. As evident, variation of intensity ratios implies a change in the overall emission color. Table 3 enlists the intensity ratios at different excitations and the resulting color of emitted light. For the $I_{420}:I_{612}$ ratio of 0.87 or less, the emitted color is strong red.

3.3.2. Emission and excitation spectra of CdS10 sample

CdS10 revealed broad emission bands around 425 and 675 nm when excited at 350 nm and 460 nm respectively, as shown in Fig. 8 (a). Based on that, excitation spectra were measured monitoring the emissions at 425 and 675 nm, shown in Fig. 8(b). Both of the spectra show a broad excitation band having a plateau region from 300 to 460 nm, with a bump around 400 nm. As the excitation spectra do not show any distinct peak position, the CdS-doped sample was excited at several wavelengths located on the plateau region of the excitation spectra to seek emission variations. Fig. 8(a) shows the emission spectra of sample CdS10 at different excitations (305, 317, 350 and 460 nm). For excitation wavelengths ≤ 350 nm, two distinct broad emission bands were observed in the violet-blue and red spectral regions. When excited at 460 nm, only the red emission band is detected. The position of the red emission band

Table 3
Intensity ratio of blue and red emission with varying excitation.

λ_{exc}	I_{612}/I_{420}	I_{420}/I_{612}	Emitted color
300	1.14	0.88	
305	0.75	1.34	
310	0.45	2.29	
315	0.66	1.12	
320	0.93	1.07	
325	0.40	2.47	
330	0.18	5.43	
335	0.11	9.08	
340	0.09	11.43	
345	0.08	11.86	
350	0.08	11.65	
355	0.16	6.18	
360	1.95	0.51	
365	0.79	1.26	
370	0.97	1.03	
375	4.17	0.24	
380	6.52	0.15	
385	4.74	0.21	
390	7.14	0.14	
395	22.16	0.05	

(675 nm) is the same for all the excitations, while the peak position of the band at the shorter wavelength region exhibits red shift with increasing excitation wavelength.

The observed broad emission bands are actually the result of overlapping bands which arise due to the presence of deep defects or trap states present in CdS crystals indicated as P₁, P₂, P₃, P₄, P₅, and P₆. Fig. 9 shows a schematic diagram of different electronic transitions taking place in CdS NPs of different particle sizes. The defect states are marked as 1, 2, 3 for smaller CdS NPs and 4,5 for relatively larger NPs. The peak marked as P₁, observed at 350 nm is related to electron-hole recombination of the relatively small size NPs. P₂ (390 nm), P₃ (405 nm) and P₄ (420 nm) are due to the defect states marked as 1, 2 and 3 respectively. Peaks P₅ (636 nm) and P₆ (675 nm) appear due to transitions from the

defect states marked as 4 and 5, respectively, in the larger NPs [39–41].

The red shifting of the emission band at violet-blue region can be attributed to the presence of QDs of different sizes. As the nature of quantum confinement indicates, the band gap increases with the decrease in particle size and vice versa. The generation and growth of the semiconductor QDs take place during the melting and annealing stages. Thus, they are uncontrolled processes generating particles of several sizes. So, the presence of very small particles having a size of a few nanometers is as probable as of bigger particles, exhibiting bulk-like properties. For smaller particles, the gap between the valence and conduction band varies due to the quantization of the energy levels. As result, for particles of different sizes, the band gap has different values. When the sample is excited with higher energy at the UV region, the

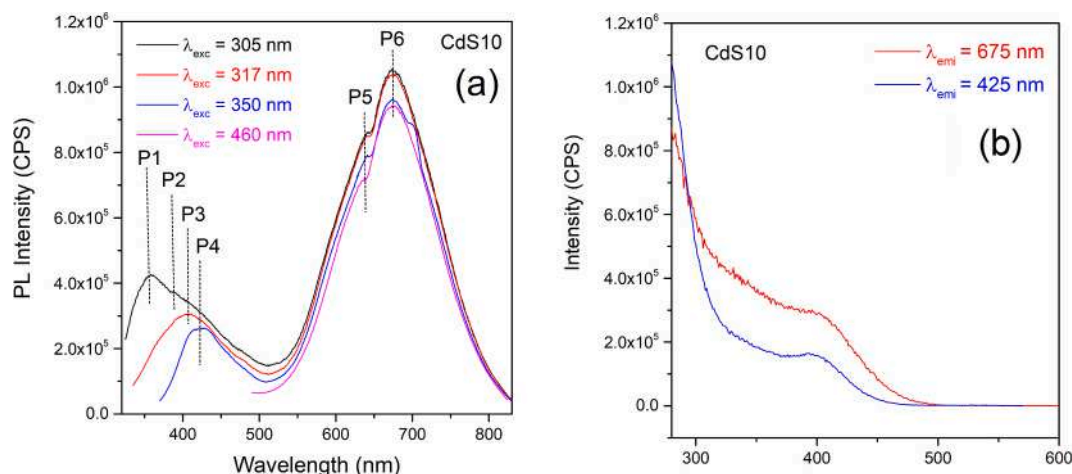


Fig. 8. (a) Emission spectra of CdS10 at different excitation wavelengths, (b) excitation spectra of CdS10 monitoring emissions at 425 and 675 nm wavelengths.

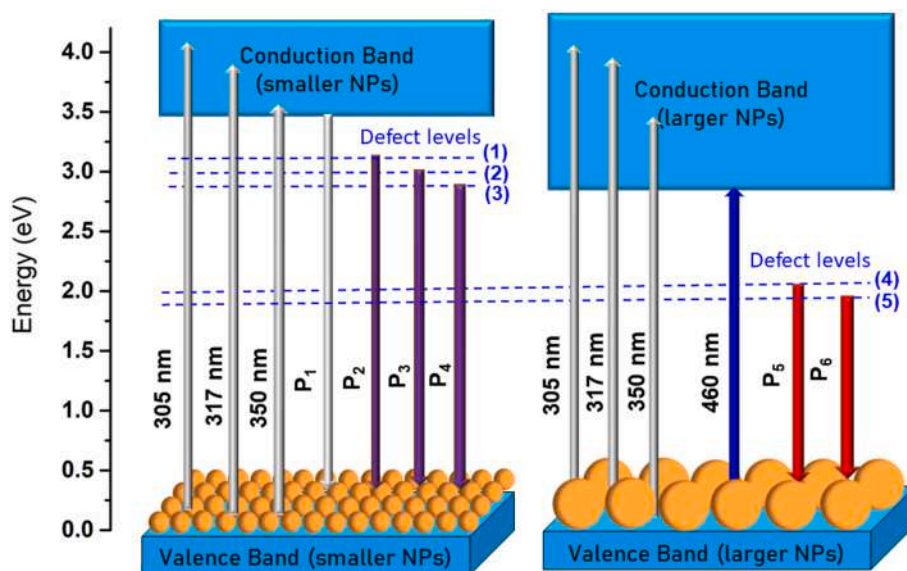


Fig. 9. Schematic diagram of CdS energy levels showing the mechanism of emission from different sizes of CdS nanoparticles [transitions based on 39–41].

absorption takes place selectively according to the size of the NPs. When excitation is 305 nm, very small NPs absorb and emit at shorter wavelengths (P₁ and P₂), which cannot be observed in the case of other excitations. When excited at relatively longer wavelengths 317 and 350 nm, relatively larger NPs absorb and emit at P₅ and P₆. For all these excitations, the position and intensity of the broad emission band in the red region remain unchanged. This indicates the presence of larger bulk-like CdS particles, which can only emit at longer wavelengths. For bigger particles, the band gap is smaller, so the radiative emissions take place from defect levels located much below the defect states of the smaller NPs. As a result, the emission at P₅ and P₆ are observed due to the transitions from defect levels 4 and 5 to the valence band. As all the larger particles act as bulk material, there is no variation in the band gap value. All of them exhibit emission at the same position (636 and 675 nm) [39–41].

3.3.3. Emission and excitation spectra of Eu³⁺/CdS co-doped glasses

When excited at 393 nm, all the Eu/CdS co-doped glasses show bright orange luminescence like the Eu-doped glass. Fig. 10 shows the PL emission spectra of all Eu and Eu/CdS doped glasses excited at 393 nm. The band positions are the same as Eu10 as shown as Fig. 3(a). It is evident from the figure that there is a considerable increase in PL

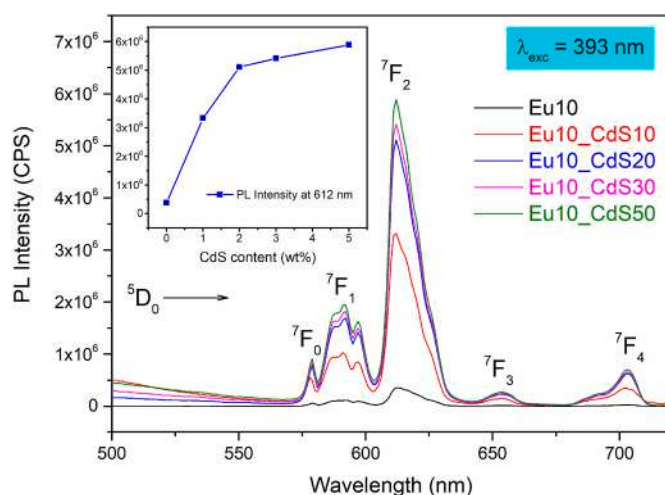


Fig. 10. PL emission spectra of Eu³⁺-doped and Eu/CdS co-doped glasses at 393 nm excitation, inset shows variation of PL intensity at 612 nm as a function of CdS content.

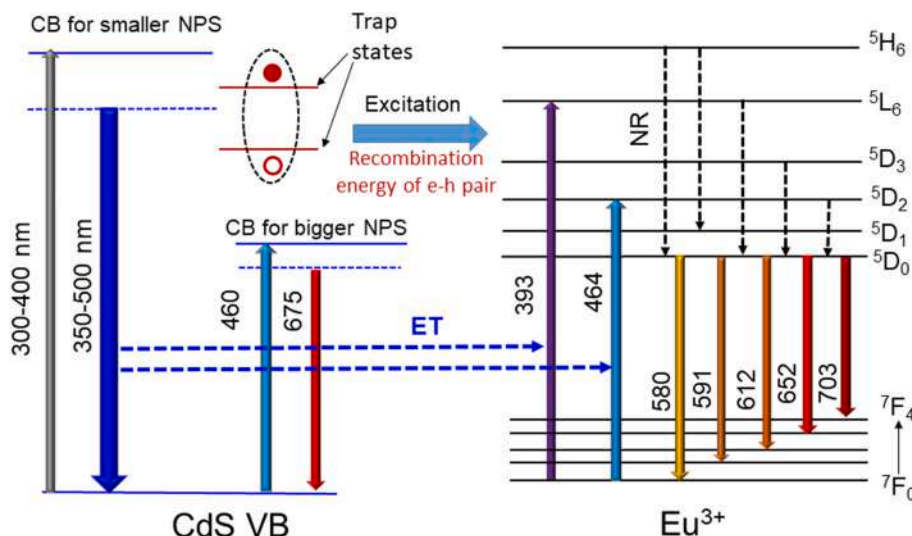


Fig. 11. Schematic energy level diagram of CdS and Eu^{3+} showing the energy transfer mechanism from CdS to Eu^{3+} leading to the Eu^{3+} PL enhancement (transitions based on [9,20–26,41–48]).

intensity from Eu10 to all the Eu/CdS co-doped glasses. The inset shows the variation in PL intensity with CdS concentration. It is observed an intensity increase of more than 10-fold from Eu10 to Eu10_CdS10. This increase continues with increasing CdS content, while the rate of enhancement slows down. The sample Eu10_CdS50 with maximum CdS content (5 wt%) show the maximum PL emission, which is around 20-fold higher than for the Eu10 sample.

This enhancement is obviously due to the presence of CdS nanoparticles in the glass. The larger the CdS concentration is, the larger is the observed enhancement effect. The mechanism of enhancement involves two pathways, (1) reabsorption of emitted light from CdS, by Eu^{3+} ions, (2) Energy transfer from CdS NPs to Eu^{3+} by electron-hole recombination mechanism [9,20–26,41–48]. Fig. 11 represents the enhancement mechanism showing the energy transfer mechanisms.

When the Eu/CdS co-doped glasses are excited at 393 nm, Eu^{3+} ions are directly excited and display their characteristic emissions. As CdS has a broad excitation band up to 450 nm, CdS also absorbs at 393 nm and gives a broad emission band ranging from 350 to 500 nm. That emission is then re-absorbed by Eu^{3+} at 393 and 464 nm, which leads to increased emission from Eu^{3+} .

Another important observation from Fig. 10, is that there is no emission band found for Eu/CdS co-doped glasses, around 675 nm, as expected from CdS QDs. The broad emission band, which is observed for CdS10 in the red region, peaking around 675 nm for any excitations between 300 and 460 nm, totally disappears in Eu/CdS co-doped glasses. An intense enhancement is found in the Eu^{3+} emissions. These two occurrences are interrelated through an energy transfer process from CdS NPs to Eu^{3+} , involving the following steps:

1. Eu^{3+} introduces isoelectronic acceptor-like electron (AE) trap states below the conduction band of CdS. It involves the isoelectronic AE trap capturing an electron, which makes it negatively charged.
2. A hole is then bound by the resulting Coulomb potential.
3. The recombination energy of the bound electron-hole pair is used to bring the electrons of Eu^{3+} ion from the ground state $7F_0$ to the excited states in an Auger process involving the electrons in the 4f-electron shell.
4. The excess energy is released by generation of (local) phonons.

This energy transfer process from CdS nanoparticles to Eu^{3+} is also responsible for the disappearance of the broad emission band at 675 nm, as well as, for the enhancement in all the emission bands of Eu^{3+} . This kind of energy transfer has previously been reported in different

semiconductor-rare earth co-doped glasses [20–26,41–48].

It is to be noted that, as Eu^{2+} does not absorb at 393 nm, there is no involvement of Eu^{2+} ions upon 393 nm excitation. The mechanism of energy transfer gets much more complex when Eu^{2+} is involved. Fig. 12 shows the emission spectra of the samples excited at 317 nm. All of the samples presented a broad emission band all over the violet-blue region (from 380 to 550 nm) centered around 430 nm and several sharp peaks in the range from 570 to 700 nm. The sharp peaks in the longer wavelength regions are attributed to the $5D_0$ to $7F_{1-4}$ levels of Eu^{3+} . The broad band in 380–550 nm region may have contributions from both Eu^{2+} and CdS QDs.

To show the comparison among the Eu and CdS-singly doped and Eu/CdS co-doped glasses, their PL spectra, with excitation at 317 nm, are shown in Fig. 13. The intense increase in the intensity of all the emission bands of Eu10, is evident when comparing the PL spectra of Eu10 and Eu10_CdS10. The maximum enhancement, observed for the

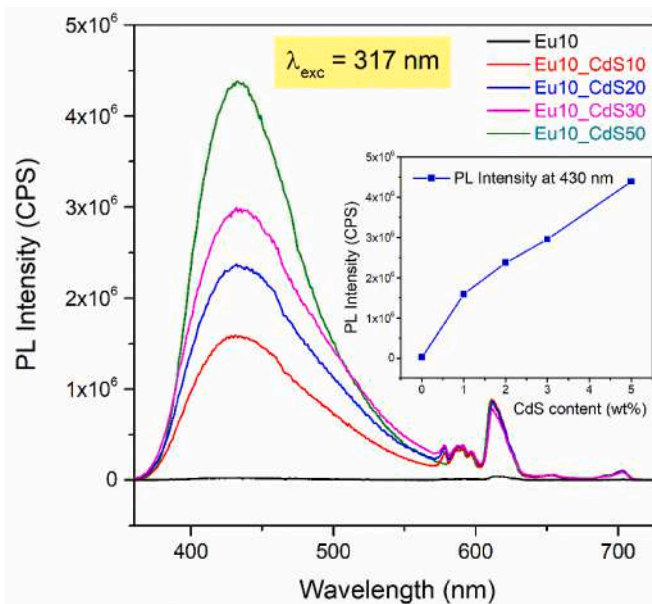


Fig. 12. PL emission spectra of Eu-doped and Eu/CdS co-doped glasses, with excitation at 317 nm excitation. The inset shows the variation of PL intensity at 430 nm as a function of CdS content.

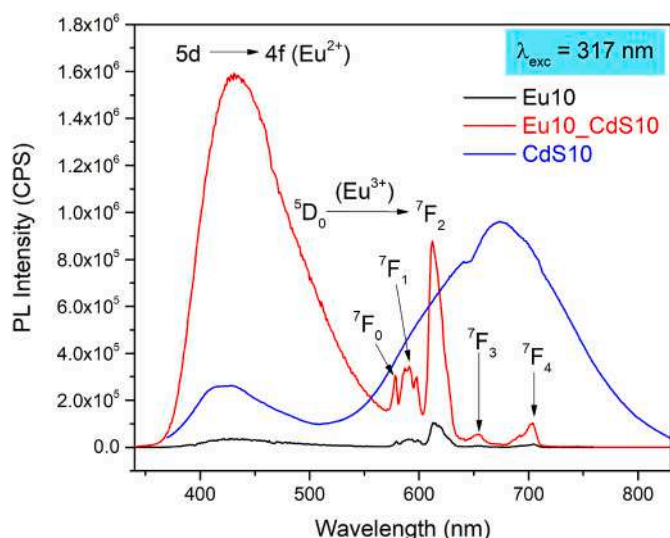


Fig. 13. PL emission spectra of Eu10, CdS10 and Eu10_CdS10 samples upon excitation at 317 nm.

broad emission band peaking around 430 nm, is around 70-fold, along with a 10-fold increase in the 612 nm emission. It should be noted that this amount of enhancement is substantially higher compared to previously reported Eu/CdS co-doped systems [19–26]. As observed in the case of 393 nm excitation, here also the broad emission band of CdS at 675 nm, disappears. These enormous increase in PL intensity in Eu^{2+} and Eu^{3+} and the disappearance of emission band in CdS are due to a complex energy transfer among the three species [33–38], represented schematically in Fig. 14.

Fig. 14 represents the schematic energy level diagram showing the energy transfer among the three species which results in the PL enhancement. As explained earlier, at 317 nm excitation, both Eu^{2+} and CdS absorb and present a broad emission band around 350–500 nm. That energy gets absorbed by Eu^{3+} which enhances its characteristic emissions in the 570–700 nm range. The energy transfer from CdS takes place through the electron-hole recombination process caused by the formation of acceptor-like trap states in CdS. That energy is transferred to both Eu^{2+} and Eu^{3+} species resulting in enhanced emission. The intensity enhancement of the band at 380–500 nm is much more pronounced due to: (1) CdS QDs has been observed to emit in that range when excited at 317 nm, so there is a possible contribution from CdS NPs to that emission band; (2) there is only a weak excitation band at 317 nm

for Eu^{3+} , while the broad excitation band for Eu^{2+} peaks near 317 nm. Thus, the direct absorption of light at 317 nm is much more intense for Eu^{2+} than for Eu^{3+} , resulting in higher enhancement in the Eu^{2+} emission.

Eu^{3+} has a very weak excitation band at 317 nm due to ${}^7\text{F}_0 \rightarrow {}^5\text{H}_6$ transition. That is why the emission for Eu^{3+} in 570–700 nm region is also very weak in Eu10. But in the presence of CdS QDs, such band intensity is 10-times magnified upon the same excitation wavelength. This increase clearly proves the occurrence of energy transfer to Eu^{3+} from the other two species. The disappearance of the large emission band of CdS at 675 nm, again demonstrates the efficiency of the energy transfer process.

3.3.4. Variation with slit width – search for white light

During this work, it was observed that Eu/CdS co-doped glasses showed prominent emission bands in the blue and red areas. The intensities of the broad band in the violet-blue region from Eu^{2+} and CdS and the sharp bands in the orange-red from Eu^{3+} region varied significantly with the excitation slit width, showing different colors of the emitted light. So, the variation of the slit width was systematically investigated, in the search of a pure white light.

PL spectra have been recorded for the Eu10_CdS10 sample at 387 nm excitation by varying the excitation slit width from 1 nm to 14 nm. The excitation wavelength was chosen at 387 nm because it is in the middle ground between 393 nm - for which the Eu^{3+} absorption is very strong, and 380 nm - up to which the excitation band of Eu^{2+} extends. So, this wavelength only excites CdS and Eu^{3+} , not involving the Eu^{2+} ions. The sharp peaks from 570 to 700 nm appear, as expected from Eu^{3+} . The broad band from 420 to 530 nm peaking around 450 nm is due to the CdS QDs. As the excitation wavelength is outside of the Eu^{2+} excitation range and Eu^{2+} does not emit at 450 nm, this emission band definitely originates from CdS. As explained earlier, with increasing excitation wavelength, the emission band of CdS shows a red shift, due to the existence of CdS QDs in the glass in a wide size range and the implicit change in effective band gap that accompanies particle size variations. Here, with 387 nm excitation, the peak of the emission band appears to be at 450 nm. The intensity ratio of these two bands changes a lot depending on the excitation slit width. To compare the ratios, the spectra have been normalized by the peak intensity at 612 nm.

From Fig. 15, it is evident that the intensity at 450 nm increases with decreasing slit width. It is also interesting to notice that the hole at 464 nm gets deeper and deeper with a narrower slit. At larger slit widths, the excitation wavelength shifts closer to 393 nm (which corresponds to the most intense excitation band for Eu^{3+}), allowing more efficient excitations and thus increasing the emission intensity at 612 nm. As the

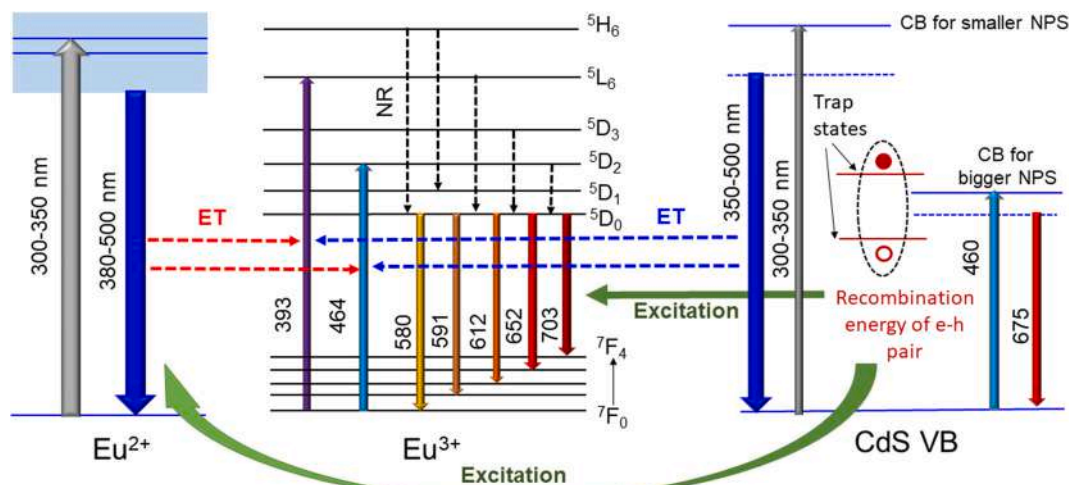


Fig. 14. Schematic energy level diagram of Eu^{2+} , Eu^{3+} and CdS showing the energy transfer mechanism for PL enhancement.

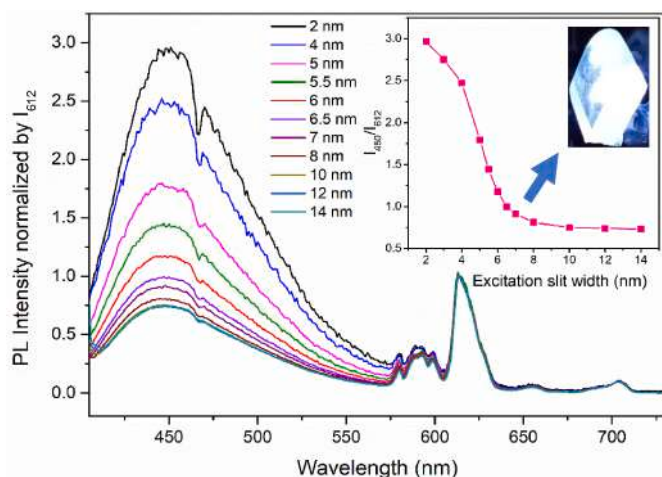


Fig. 15. PL spectra of Eu10_CdS10 sample (normalized by the intensity at 612 nm) at 387 nm excitation. The inset shows the change in intensity ratio with varying excitation slit width.

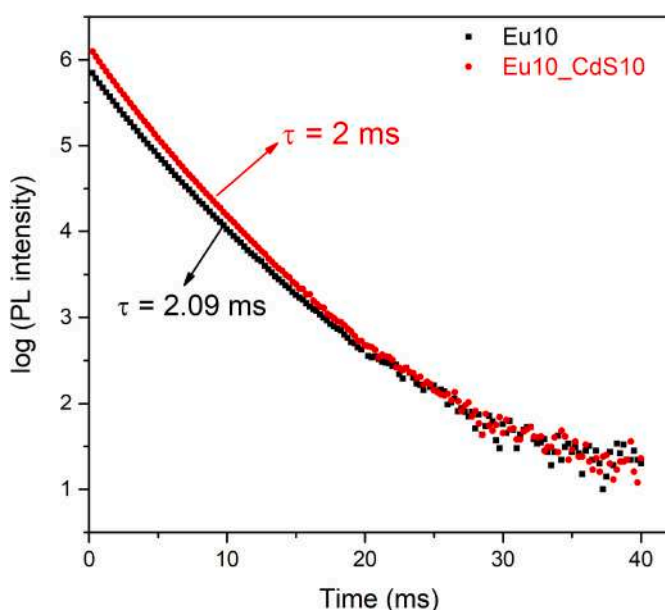


Fig. 16. Representative luminescence decay curves of Eu10 and Eu10_CdS10 for 393 nm excitation and emission at 612 nm.

excitation for CdS NPs remains the same, the intensity at 450 nm remains almost the same. When the slit is gradually closed, the excitation wavelength distances from 393 nm thus decreasing the direct excitation of Eu^{3+} ions. Eu^{3+} ions then absorb the required excitation energy from the emission band of CdS, mostly at 464 nm. The smaller the slit width, the more absorption occurs by Eu^{3+} , causing the hole to get deeper. This is another evidence of energy transfer from CdS to Eu^{3+} . The inset of Fig. 16 shows the intensity ratio of emissions at 450 and 612 nm, as a function of slit width. The ratio changes a lot, which indicates the wide variation of the emitted color. For smaller slit width, it emits blue and at larger width, it emits red. Around slit width 6–7 nm, the ratio becomes close to 1, at that point the color of the emitted light becomes almost pure white. Inset shows the image of white light emission.

3.4. Fluorescence lifetimes

The most intense PL emission was observed at 612 nm, when excited at 393 nm, for all the Eu-containing samples. This is the most prominent

emission band originating from Eu^{3+} ion. That is why the fluorescence lifetimes have been measured for this transition. Excited state lifetime values were determined from the luminescence decay curves for all the samples by monitoring the emission at 612 nm, at 393 nm excitation. Fig. 16 shows the representative decay curves of Eu10 and Eu10_CdS10 samples. The lifetime values for all samples were calculated to be in the range of 1.83–2.09 ms. The value of lifetimes did not show much variation with change in dopant concentrations up to the levels studied. Generally, in presence of an energy transfer process, a decrease in lifetime (based on luminescence decay) of the donor species is expected whereas an increase in rise time of the acceptor species could (not necessarily) be observed. Therefore, the recommended experiment would be to measure the lifetime decay of the CdS QDs in the presence of the Eu species. However, this measurement was not possible because, as described and explained earlier (Fig. 13), in glasses containing both Eu ions and CdS QDs, the emission of the latter disappears due to the very efficient energy transfer.

4. Conclusions

CdS QDs in the size range of 5–20 nm have been successfully generated into chloroborosilicate glass, for the first time, using the one-step melt-quench technique. The CdS-doped glass showed two broad emission bands, peaking around 430 and 675 nm, originating from various electronic transitions involving the defect and trap states in CdS crystal. The band in the lower wavelength region shows a red shift with increasing excitation wavelength, which proves the quantum confinement effect in CdS QDs. Co-doping the glasses with europium resulted in the generation of both divalent and trivalent Eu ions. The existence of an energy transfer process involving the CTB and the different energy levels of Eu^{2+} and Eu^{3+} ions has been proven. Also, the color of the emission was found to vary largely with excitation wavelength, which confirms the presence of both Eu^{2+} and Eu^{3+} . Eu/CdS co-doped glasses showed intense enhancements in $\text{Eu}^{3+}/\text{Eu}^{2+}$ emissions, of 20 and up to 70 times, at 393 and 317 nm excitations, respectively. This is considerably higher compared to previously reported Eu/CdS co-doped systems [19–26]. This enhancement is attributed to a complex energy transfer occurring between Eu^{2+} , Eu^{3+} , and CdS QDs, reported for the first time in a $\text{Eu}^{2+}/\text{Eu}^{3+}/\text{CdS}$ -co-doped glass system. The enhancement effect increases almost linearly with CdS content. The Eu/CdS co-doped glass showed variation in emission color with variation in excitation slit, giving pure white emission at 387 nm excitation and 6–7 nm slit width, which is also a novel finding from an Eu/CdS doped glass. The fluorescence lifetimes for 612 nm emission were measured to be in the range of 1.83–2.09 ms and do not vary significantly with dopant concentrations.

Author statement

All persons who meet authorship criteria are listed as authors, and all authors certify that they have participated sufficiently in the work to take public responsibility for the content, including participation in the concept, design, analysis, writing, or revision of the manuscript. Furthermore, each author certifies that this material or similar material has not been and will not be submitted to or published in any other publication before its appearance in the Journal of Luminescence.

Declaration of competing interest

The authors declare that they have no known competing financial interests or personal relationships that could have appeared to influence the work reported in this paper.

Acknowledgements

The authors acknowledge the financial support of Center for

Research, Technology and Education in Vitreous Materials (CeRTEV, Fundação de Amparo a Pesquisa do Estado de São Paulo), through CEPID program, process number 2013/00793-6. NS acknowledges the financial support from Fapesp post-doctoral fellowship process number 2018/04113-8.

References

- [1] M.V. Kovalenko, et al., Prospects of nanoscience with nanocrystals, *ACS Nano* 9 (2015) 1012–1057.
- [2] C.D.M. Donega (Ed.), *Nanoparticles. Workbooks of Nanoscience*, Springer Berlin Heidelberg, 2014.
- [3] C.B. Murray, D.J. Norris, M.G. Bawendi, Synthesis and characterization of nearly monodisperse CdE (E = sulfur, selenium, tellurium) semiconductor nanocrystallites, *J. Am. Chem. Soc.* 115 (1993) 8706–8715.
- [4] C. Dey, B. Karmakar, *Enhanced green and orange photoluminescence of nanostructured CdS in glass nanocomposites by energy transfer from Ho³⁺ and Eu³⁺ ions*, *Semicond. Sci. Technol.* 32 (2017), 015003.
- [5] S. Kim, et al., Highly luminescent InP/GaP/ZnS Nanocrystals and their application to blue light-emitting diodes, *J. Am. Chem. Soc.* 134 (2012) 3804–3809.
- [6] S. Suresh, Studies on the dielectric properties of CdS nanoparticles, *Appl. Nanosci.* 4 (2014) 325–329.
- [7] M.A. Correa-Duarte, M. Giersig, L.M. Liz-Marz'án, Stabilization of CdS semiconductor nanoparticles against photodegradation by a silica coating procedure, *Chem. Phys. Lett.* 286 (1998) 497–501.
- [8] N. Thanh, L. Green, Functionalisation of nanoparticles for biomedical applications, *Nano Today* 5 (2010) 213–230.
- [9] B. Julian, J. Planelles, E. Cordoncillo, P. Escrivano, P. Aschehoug, C. Sanchez, B. Viana, F. Pelle, *Eu³⁺-doped CdS nanocrystals in SiO₂ matrices: one-pot sol-gel synthesis and optical characterization*, *J. Mater. Chem.* 16 (2006) 4612–4618.
- [10] H. Minti, M. Eyal, R. Reisfeld, G. Berkovic, Quantum dots of cadmium sulfide in thin glass films prepared by sol-gel technique, *Chem. Phys. Lett.* 183 (1991) 277.
- [11] L. Spanhel, E. Arpac, H.M. Schmidt, Semiconductor clusters in the sol-gel process: synthesis and properties of CdS nanocomposites, *J. Non-Cryst. Solids* 147–148 (1992) 657.
- [12] M. Zelner, H. Minti, R. Reisfeld, H. Cohen, R. Tenne, Preparation and characterization of CdS films synthesized in situ in zirconia Sol-gel matrix, *Chem. Mater.* 9 (1997) 2541.
- [13] A.A. Ansari, A.K. Parchur, B. Kumar, S.B. Rai, *Highly aqueous soluble CaF₂: Ce/Tb nanocrystals: effect of surface functionalization on structural, optical band gap, and photoluminescence properties*, *J. Mater. Sci. Mater. Med.* 27 (2016) 178.
- [14] M. Odziomek, F. Chaput, F. Lerouge, M. Sitarz, S. Parola, Highly luminescent YAG: Ce ultra-small nanocrystals, from stable dispersions to thin films, *J. Mater. Chem. C* 5 (2017) 12561–12570.
- [15] Y. Wu, S. Lin, J. Liu, Y. Ji, J. Xu, L. Xu, K. Chen, *Efficient up-conversion red emission from TiO₂: Yb, Er nanocrystals*, *Opt Express* 25 (2017) 22648–22657.
- [16] H. He, Y. Zhang, Q. Pan, G. Wu, G. Dong, J. Qiu, *Controllable synthesis of Zn₂GeO₄: Eu nanocrystals with multi-color emission for white light-emitting diodes*, *J. Mater. Chem. C* 3 (2015) 5419–5429.
- [17] J.F. Gao, J.H. Yang, X.Y. Zhang, J. Zhao, X.W. Liu, B.F. Shi, *Synthesis and fluorescence properties of CdTe: Eu³⁺ nanocrystals and core-shell SiO₂-coated CdTe: Eu³⁺ nanospheres*, *Rare Met.* 38 (2019) 989–995.
- [18] J.Y. Parka, E.J. Jeona, Y.H. Choa, B.S. Kim, Optical and structural properties of ZnSe quantum dot with europium, *J. Lumin.* 208 (2019) 145–149.
- [19] J.P. Arag, E. Cordoncillo, R.A.S. Ferreira, L.D. Carlos, P. Escrivano, Synthesis, characterization and optical studies on lanthanide-doped CdS quantum dots: new insights on CdS → lanthanide energy transfer mechanisms, *J. Mater. Chem.* 21 (2011) 1162–1170.
- [20] F.B. Slimen, Z. Zaaboub, M. Haouari, N.B.H. Mohamed, H.B. Ouada, S. Chausseudent, N. Gaumer, *Effect of CdS nanocrystals on the photoluminescence of Eu³⁺-doped silicophosphate sol gel glass*, *RSC Adv.* 7 (2017) 14552.
- [21] P.M. Tan, N.X. Ca, N.T. Hien, H.T. Van, P.V. Do, L.D. Thanh, V.H. Yen, V.P. Tuyen, Y. Peng, P.T. Tho, New insights on the energy transfer mechanisms of Eu-doped CdS quantum dots, *Phys. Chem. Chem. Phys.* 22 (2020) 6266.
- [22] T. Hayakawa, S.T. Selvan, M. Nogami, *Energy transfer between Eu³⁺ ions and CdS quantum Dots in sol-gel derived CdS/SiO₂: Eu³⁺ gel*, *J. Sol. Gel Sci. Technol.* 19 (2000) 779–783.
- [23] L. Bokatiál, S. Rai, *Photoluminescence and energy transfer Study of Eu³⁺ Codoped with CdS Nanoparticles in silica glass*, *J. Fluoresc.* 22 (2012) 505–510.
- [24] S.T. Selvan, T. Hayakawa, M. Nogami, *Enhanced fluorescence from Eu³⁺-doped silica gels by adsorbed CdS nanoparticles*, *J. Non-Cryst. Solids* 291 (2001) 137–141.
- [25] T. Hayakawa, S.T. Selvan, M. Nogami, *Influence of adsorbed CdS nanoparticles on ⁵D₀ → ⁷F_J emissions in Eu³⁺-doped silica gel*, *J. Lumin.* 87–89 (2000) 532–534.
- [26] M. Shkir, I.M. Ashraf, K.V. Chandekar, I.S. Yahia, A. Khan, H. Algarni, S. AlFaify, A significant enhancement in visible-light photodetection properties of chemical spray pyrolysis fabricated CdS thin films by novel Eu doping concentrations, *Sensor. Actuator.* 301 (2020) 111749.
- [27] N. Shasmal, A.R. Molla, B. Karmakar, *Synthesis and characterization of chloroborosilicate glasses in the K₂O–BaO–Al₂O₃–B₂O₃–SiO₂–BaCl₂ system*, *J. Non-Cryst. Solids* 398–399 (2014) 32–41.
- [28] N. Shasmal, B. Karmakar, Localized surface plasmon absorption and photoluminescence of in situ-generated nano silver in a novel chloroborosilicate glass and glass ceramics, *Plasmonics* 10 (2015) 191–202.
- [29] N. Shasmal, K. Pradeep, B. Karmakar, *Enhanced photoluminescence up and downconversions of Sm³⁺ ions by Ag nanoparticles in chloroborosilicate glass nanocomposites*, *RSC Adv.* 5 (2015) 81123.
- [30] N. Shasmal, B. Karmakar, Enhancement of photoluminescence in white light emitting glasses by localized surface plasmons of Ag and Au nanoparticles, *Chem. Phys. Lett.* 754 (2020) 137713.
- [31] N. Shasmal, B. Karmakar, *Synthesis of transparent chloroborosilicate nanoglass-ceramics: Crystallization and growth mechanism of BaCl₂ nanocrystals*, *J. Asian Ceram. Soc.* 3 (2015) 390–401.
- [32] W.T. Carnall, P.R. Fields, K. Rajnak, *Electronic energy Levels of the trivalent lanthanide aquo ions. IV. Eu³⁺*, *J. Chem. Phys.* 49 (10) (1968) 4450–4455.
- [33] A. Tarafder, A.R. Molla, C. Dey, B. Karmakar, *Thermal, structural, and enhanced photoluminescence Properties of Eu³⁺-doped transparent willemite glass-ceramic nanocomposites*, *J. Am. Ceram. Soc.* 96 (8) (2013) 2424–2431.
- [34] K. Biswas, A.D. Sontakke, R. Sen, K. Annapurma, *Luminescence Properties of dual valence Eu doped nano-crystalline BaF₂ embedded glass-ceramics and Observation of Eu²⁺ → Eu³⁺ energy transfer*, *J. Fluoresc.* 22 (2012) 745–752.
- [35] Q. Yanmin, Z. Xinbo, Y. Xiao, C. Yan, G. Hai, *Photoluminescent properties of Sr₂SiO₄: Eu³⁺ and Sr₂SiO₄:Eu²⁺ phosphors prepared by solid-state reaction method*, *J. Rare Earths* 27 (2009) 323.
- [36] W. Chen, Y. Ouyang, M. Mo, H. Zhang, Q. Su, *Observation of energy transfer from Eu²⁺ to Eu³⁺ and tunable luminescence in phosphors YF₃:Eu prepared by hydrothermal method*, *J. Lumin.* 229 (2021) 117672.
- [37] A. Nag, T.R.N. Kutty, *The light induced valence change of europium in Sr₂SiO₄:Eu involving transient crystal structure*, *J. Mater. Chem.* 14 (2004) 1598.
- [38] Z. Zhang, Y. Wang, *Photoluminescence of Eu²⁺-doped CaMgSi₂xO_{6+2x} (1.00 ≤ x ≤ 1.20) Phosphors in UV-VUV region*, *J. Lumin.* 128 (2008) 383.
- [39] C. Dey, A.R. Molla, A. Tarafder, M. Mishra, G. De, M. Goswami, G.P. Kothiyal, B. Karmakar, Single-step in-situ synthesis and optical properties of ZnSe nanostructured dielectric nanocomposites, *J. Appl. Phys.* 115 (2014) 134309.
- [40] C. Dey, A.R. Molla, M. Goswami, G. Kothiyal, B. Karmakar, Synthesis and optical properties of multifunctional CdS nanostructured dielectric nanocomposites, *J. Opt. Soc. Am. B* 31 (2014) 1761.
- [41] N. Shasmal, W.J. Faria, A.S.S. Camargo, A.C.M. Rodrigues, *Enhancement in green and NIR emissions of Er³⁺ by energy transfer from ZnSe nanoparticles in borosilicate glass*, *J. Alloys Compd.* 863 (2021) 158428.
- [42] P. Chowdhury, A. Patra, *Role of dopant concentration and surface coating on photophysical properties of CdS: Eu³⁺ nanocrystals*, *Phys. Chem. Chem. Phys.* 8 (2006) 1329–1334.
- [43] [G. Jose, G. Jose, V. Thomas, C. Joseph, M.A. Ittyachen, N.V. Unnikrishnan, *Optical Characterization of Eu³⁺ Ions in CdSe nanocrystal containing silica glass*, *J. Fluoresc.* 14 (2004) 733–738.
- [44] [Y. Yu, Y. Wang, D. Chen, P. Huang, E. Ma, F. Bao, *Enhanced emissions of Eu³⁺ by energy transfer from ZnO quantum dots embedded in SiO₂ glass*, *Nanotechnology* 19 (2008), 055711.
- [45] T.T. Van Tran, T.M. Dung Cao, Quang Vinh Lam, Le Van Hieu, *Emission of Eu³⁺ in SiO₂-ZnO glass and SiO₂-SnO₂ glass-ceramic: Correlation between structure and optical properties of Eu³⁺ ions*, *J. Non-Cryst. Solids* 459 (2017) 57–62.
- [46] S. Mathew, P.R. Rejikumar, X. Joseph, N.V. Unnikrishnan, *Optical studies on Eu³⁺/ZnSe nanocrystal in silica hosts*, *Opt. Mater.* 29 (2007) 1689–1692.
- [47] E.O. Serqueira, N.O. Dantas, *Determination of the energy transfer section between CdS semiconductor quantum dots and Nd³⁺ ions*, *Opt. Mater.* 90 (2019) 252–256.
- [48] D. Chen, Y. Wang, E. Ma, F. Bao, Y. Yu, *Luminescence of an Er³⁺-doped glass matrix containing CdS quantum dots*, *Scripta Mater.* 55 (2006) 891–894.